Narrow escape problem with a mixed trap and the effect of orientation

A.E. Lindsay, T. Kolokolnikov, and J.C. Tzou

February 16, 2015

Abstract

We consider the mean first passage time (MFPT) of a two dimensional diffusing particle to a small trap with a distribution of absorbing and reflecting sections. High order asymptotic formulae for the MFPT and the fundamental eigenvalue of the Laplacian are derived which extend previously obtained results and show how the orientation of the trap affects the mean time to capture. We obtain a simple geometric condition which gives the optimal trap alignment in terms of the gradient of the regular part of a regular part of a Green's function and a certain alignment vector. We find that subdividing the absorbing portions of the trap reduces the mean first passage time of the diffusing particle. In the scenario where the trap undergoes prescribed motion in the domain, the MFPT is seen to be particularly sensitive to the orientation of the trap.

1 Introduction

We study the mean first passage time (MFPT) problem for the expected survival time of a particle undergoing a random walk in a confined two dimensional region with a small absorbing trap. Random dispersal is a fundamental transport mechanism in many physical, biological and social systems. Consequently, studies of the MFPT problem are prominent in many applications and enjoy a burgeoning presence in the recent literature. Applications involving MFPT problems include intracellular transport [1, 2], oxygen transport [3], predator-prey dynamics [4, 5], DNA sites [6, 7], and T-cell receptor (TCR) signaling [8]. Recent developments and applications of MFPT problems have been summarized in several review articles [1, 9–12].

The formulation (cf. [13, 14]) of the first passage time $w(\mathbf{x})$ of a particle starting at $\mathbf{x} \in \Omega$, reduces to the mixed Dirichlet-Neumann boundary value problem

$$D\Delta w + 1 = 0, \qquad \mathbf{x} \in \Omega; \tag{1.1a}$$

$$w = 0, \qquad \mathbf{x} \in \partial\Omega^a; \qquad \frac{\partial w}{\partial n} = 0, \qquad \mathbf{x} \in \partial\Omega^r, \tag{1.1b}$$

where D is the diffusion coefficient of the particle, $\Omega \subset \mathbb{R}^d$ is a bounded region in dimension $d = 1, 2, 3$, and $\partial\Omega^a$ and $\partial\Omega^r$ are absorbing and reflecting boundary segments, respectively. The particular focus of this article is on the two-dimensional case and the scenario where the initial locations $\mathbf{x} \in \Omega$ have the uniform distribution $\rho(\mathbf{x}) = |\Omega|^{-1}$. The average MFPT τ is then given by

$$\tau = \int_\Omega \rho(\mathbf{x})w(\mathbf{x})\,d\mathbf{x} = \frac{1}{|\Omega|}\int_\Omega w(\mathbf{x})\,d\mathbf{x}.$$

An important scenario known as the "narrow escape problem" arises when the boundary is predominately reflecting, with the absorbing region consisting of proportionately small segments located on the boundary. That is, $|\partial\Omega^a|/|\partial\Omega^r| \ll 1$ in (1.1). In this case, the absorbing segments can take the form of small boundary windows [15, 16] or a collection of small interior traps [17–19]. A common problem in chemical engineering involves the equilibrium between two gas chambers connected by a thin capillary [20]. In this case, the first passage time of gas particles to the capillary aperture in each chamber is an important quantity in
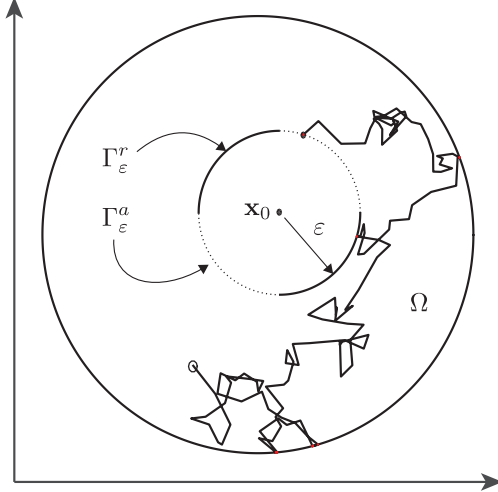
Figure 1: Schematic diagram of a bounded two-dimensional region Ω with a trap of radius ε composed of reflecting (solid lines) and absorbing (dashed lines) sections, Γ_ε^r and Γ_ε^a.

determining the time to equilibration between the two chambers. In many biologically motivated narrow escape problems, the absorbing region indicates a site on a cell surface at which a reaction of interest takes place, or a channel through which ions, proteins and RNA molecules are transported. In these cases, the surface is not uniformly absorbing, but rather features a distribution of absorbing and reflecting subdomains. For more applications, including a description of the original problem formulation by Lord Rayleigh in the context of acoustics, see [21, 22] and references therein.

An important example is the case for T-cell signaling, whereby the receptors (TCRs) at which reactions take place are formed of micro clusters distributed along the cell membrane [8, 23]. Therefore, the diffusing molecule must reach particular absorbing subdomains of the membrane to trigger a reaction. Another example is the import of proteins synthesized in the cytoplasm of a eukaryotic cell into the nucleus. The proteins must diffuse to certain sites on the nuclear envelope in order to enter the nucleus through the nuclear pore complex. See the reviews [24–26] and references therein for detailed descriptions of the mechanisms involved in nucleocytoplasmic transport.

The primary feature of these examples is that the diffusing molecules seek not only to find the trap, but must reach specific locations on the trap's boundary to complete their process. This differs from the Robin boundary condition case where the diffusing particle is absorbed with a predetermined probability once it encounters the trap and reflected otherwise (cf. [27]). In such a scenario, a circular trap retains its symmetric profile and orientation does not contribute to the MFPT. The present work focusses on the symmetry breaking effects that occur in the mixed configuration scenario where traps have non-contiguous absorbing and reflecting sections (cf. Fig. 1) with Dirichlet and Neumann boundary conditions applied on each.

In [28], first passage times are computed for a radially symmetric scenario in which the mixed configuration absorbing interior trap is circular and concentric with the outer boundary. In the present work, we investigate the more general case of an off-center trap, which breaks the symmetry and gives rise to important orientation and boundary effects on MFPT. The break in symmetry also requires different analysis techniques. We discuss both of these aspects below.

The present work considers the scenario of a single small trap Ω_ε centered at $\mathbf{x}_0$ inside a two dimensional domain Ω. The trap is expressed explicitly as $\Omega_\varepsilon = \mathbf{x}_0 + \varepsilon \Omega_0$, where Ω_0 is the geometry of the trap and the small parameter ε is the trap "radius". The boundary of the trap is composed of non-overlapping absorbing and reflecting sections, Γ_0^a and Γ_0^r so that $\partial \Omega_0 = \Gamma_0^a \cup \Gamma_0^r$ - (cf. Fig. 1). The asymmetry of the trap contributes to the MFPT and in §2 we obtain, for a bounded two dimensional region Ω, the three term asymptotic expression

$$\tau = \frac{|\Omega|}{D} \left[\frac{1}{2\pi\nu} + R_m(\mathbf{x}_0; \mathbf{x}_0) - \varepsilon(\mathbf{p} + \mathbf{b}) \cdot \nabla_{\mathbf{x}} R_m(\mathbf{x}_0; \mathbf{x}_0) \right] + \mathcal{O}(\varepsilon^2), \qquad \nu = \frac{-1}{\log \varepsilon d_0}. \qquad (1.2)$$

2

in the limit as $\varepsilon \to 0$. Each term of (1.2) encodes particular physical attributes of the problem into the MFPT. The size of the trap and its distribution of absorbing and reflecting is reflected in (1.2) by the quantity εd_0 where ε is the radius and d_0 is the "logarithmic capacitance" of the trap. The term $R_m(\mathbf{x}_0; \mathbf{x}_0)$ describes the dependence of τ on the spatial location of the trap within the confining two dimensional region Ω. The third term describes the effect on τ of trap orientation through the reflected by the vector $\mathbf{p} + \mathbf{b}$ and the quantity $\nabla_{\mathbf{x}} R_m(\mathbf{x}_0; \mathbf{x}_0)$. The three quantities $d_0, \mathbf{p}, \mathbf{b}$ satisfy related exterior problems and in certain scenarios where Ω_0 is radially symmetric, their values are calculated explicitly. The function $R_m(\mathbf{x}; \boldsymbol{\xi})$ is the regular part of the modified Neumann Green's function $G_m(\mathbf{x}; \boldsymbol{\xi})$ satisfying

$$\Delta G_m = \frac{1}{|\Omega|} - \delta(\mathbf{x} - \boldsymbol{\xi}), \qquad \mathbf{x} \in \Omega; \qquad \frac{\partial G_m}{\partial n} = 0, \quad \mathbf{x} \in \partial\Omega; \tag{1.3a}$$

$$\int_\Omega G_m \, d\mathbf{x} = 0; \qquad G_m = \frac{-1}{2\pi} \log |\mathbf{x} - \boldsymbol{\xi}| + R_m(\mathbf{x}; \boldsymbol{\xi}). \tag{1.3b}$$

In §2.1, we validate (1.2) with numerical solutions of (1.1) for the case where Ω is the unit disk. We also illustrate a "shielding effect" induced by the boundary's obstruction of the absorbing portion of the trap. This effect is unique to an off-center, mixed configuration trap, and is absent in the case of both the centered trap considered in [28], and the fully absorbing trap in [18].

The MFPT is closely related to the fundamental eigenvalue of the Laplacian [18, 27, 29], ie. the smallest $\lambda_f > 0$, satisfying the problem

$$\Delta u + \lambda u = 0, \qquad \mathbf{x} \in \Omega \setminus \Omega_\varepsilon; \qquad \int_{\Omega \setminus \Omega_\varepsilon} u^2 \, d\mathbf{x} = 1; \tag{1.4a}$$

$$\frac{\partial u}{\partial n} = 0, \quad \text{on} \quad \partial\Omega; \tag{1.4b}$$

$$u = 0, \quad \text{on} \quad \Gamma_\varepsilon^a, \qquad \frac{\partial u}{\partial n} = 0 \quad \text{on} \quad \Gamma_\varepsilon^r, \tag{1.4c}$$

where $\partial\Omega_\varepsilon = \Gamma_\varepsilon^r \cup \Gamma_\varepsilon^a$. For example, the detailed matched asymptotic study of [16] determined the relationship

$$\tau = \frac{1}{D\lambda_0(\nu)} + \mathcal{O}(\nu^2), \tag{1.5}$$

where in terms of the fundamental eigenvalue λ_f of (1.4),

$$\lambda_f = \lambda_0(\nu) + \mathcal{O}(\varepsilon\nu), \qquad R_h(\mathbf{x}_0; \mathbf{x}_0, \lambda_0(\nu)) = \frac{-1}{2\pi\nu}. \tag{1.6}$$

In this formulation, $\lambda_0(\nu)$ is a term which "sums the logs" and the function $R_h(\mathbf{x}; \boldsymbol{\xi}, \lambda)$ is the regular part of the Helmholtz Green's function $G_h(\mathbf{x}; \boldsymbol{\xi}, \lambda)$ satisfying

$$\Delta G_h + \lambda G_h = -\delta(\mathbf{x} - \boldsymbol{\xi}), \qquad \mathbf{x} \in \Omega; \qquad \frac{\partial G_h}{\partial n} = 0, \quad \mathbf{x} \in \partial\Omega; \tag{1.7a}$$

$$G_h = \frac{-1}{2\pi} \log |\mathbf{x} - \boldsymbol{\xi}| + R_h(\mathbf{x}; \boldsymbol{\xi}, \lambda). \tag{1.7b}$$

It is clear from (1.5) that maximizing λ_0 minimizes τ and vice versa. However, the definition of λ_0 in (1.6) implies this is true only up to quantities d_0 and $\mathbf{x}_0$ and does not take into account trap orientation. To examine the relationship between optimization of τ and λ_f once orientation information is included, we obtain in §3 the asymptotic formula

$$\lambda_f = \lambda_0(\nu) + \varepsilon \frac{(\mathbf{p} + \mathbf{b})}{\langle G_h, G_h \rangle} \cdot \nabla_{\mathbf{x}} R_h(\mathbf{x}_0; \mathbf{x}_0, \lambda_0) + \mathcal{O}(\varepsilon^2), \qquad \nu = \frac{-1}{\log \varepsilon d_0}, \tag{1.8}$$

for the fundamental eigenvalue of (1.4) in the limit $\varepsilon \to 0$. Here $\langle f, g \rangle = \int_\Omega fg \, d\mathbf{x}$. The leading order term of (1.8), previously obtained in ([18, 27]), depends on the shape of Ω_0 and the configuration of absorbing and reflecting segments via the parameter d_0 determined by (3.25). The higher order correction term captures the effect of trap alignment on the fundamental eigenvalue.

3

The explicit formulae for (1.2) given in (1.8) shows that the alignment vector $(\mathbf{p} + \mathbf{b})$ should be co-linear with the gradient of the regular parts R_m and R_h in order to minimize the time to capture τ and maximize λ_f respectively. In §3.1, the validity of the asymptotic formula (1.8) is verified on several test cases and the trap alignment is shown to have a significant effect on the efficacy of the trap. We remark that the inclusion of the higher order terms in formula (1.8) results in approximations for τ and λ_f which are accurate for much larger ranges of values of ε than the leading order term (1.6) alone.

In §4 we investigate the effect of fragmenting the trap into multiple absorbing and reflecting windows and determine an effective logarithmic capacitance in the limit of small absorbing window size. In particular, for a fixed total absorbing fraction, we identify a homogenized limiting problem for a large number of periodically arranged absorbing windows. Finally, we numerically investigate the combined effect of trap orientation on a trap undergoing prescribed circular motion in the domain.

2 Calculation of the mean first passage time

This section is focused on obtaining an asymptotic solution $w(\mathbf{x}; \varepsilon)$ for equation (1.1) in two dimensions as $\varepsilon \to 0$ accurate to $\mathcal{O}(\varepsilon)$. This level of accuracy is required to incorporate information regarding the alignment of the trap into an expression for the MFPT. We formulate an expansion

$$w(\mathbf{x}; \varepsilon) = w_0(\mathbf{x}; \nu) + \varepsilon w_1(\mathbf{x}; \nu) + \mathcal{O}(\varepsilon^2), \qquad \nu = \frac{-1}{\log \varepsilon d_0}, \tag{2.9}$$

for the solution in the outer region. In the vicinity of the trap, a local solution is sought in terms of the variable $\mathbf{y} = \varepsilon^{-1}(\mathbf{x} - \mathbf{x}_0)$ and the canonical harmonic function $v_c(\mathbf{y})$ with mixed Neumann-Dirichlet boundary conditions satisfying

$$\Delta v_c = 0, \qquad \mathbf{y} \in \mathbb{R}^2 \setminus \Omega_0; \tag{2.10a}$$

$$v_c = 0 \quad \text{on} \quad \Gamma_0^a, \qquad \frac{\partial v_c}{\partial n} = 0 \quad \text{on} \quad \Gamma_0^r; \tag{2.10b}$$

$$v_c(\mathbf{y}) = \log|\mathbf{y}| - \log d_0 + \frac{\mathbf{p} \cdot \mathbf{y}}{|\mathbf{y}|^2} + \mathcal{O}\left(\frac{1}{|\mathbf{y}|^2}\right), \qquad |\mathbf{y}| \to \infty, \tag{2.10c}$$

where $\partial \Omega_0 = \Gamma_0^r \cup \Gamma_0^a$. The far field behavior (2.10a) of v_c features parameters d_0 and $\mathbf{p}$, the logarithmic capacitance and dipole vector, respectively. In the setup displayed in Fig. 2, where Ω_0 is the unit disk and the trap is absorbing apart from a segment of arc length 2α orientated at an angle ϕ, the values of d_0 and $\mathbf{p}$ are calculated in Appendix A to be

$$d_0 = \exp\left(-\frac{a_0}{2}\right), \qquad a_0 = \frac{2\sqrt{2}}{\pi} \int_0^\alpha \frac{u \sin \frac{u}{2}}{\sqrt{\cos u - \cos \alpha}} \, du. \tag{2.11a}$$

$$\mathbf{p} = a_1 \begin{bmatrix} \cos \phi \\ \sin \phi \end{bmatrix}, \qquad a_1 = a_0 \cos^2 \frac{\alpha}{2} + \frac{2\sqrt{2}}{\pi} \int_0^\alpha u \sin \frac{u}{2} \sqrt{\cos u - \cos \alpha} \, du. \tag{2.11b}$$

In the case of an all absorbing circular trap for which $\alpha = 0$, the parameter values are $a_0 = 0$, $d_0 = 1$ and $a_1 = 0$. The all-reflecting case is singular and corresponds to a divergence of the MFPT and the integral formula for a_0 in (2.11a). The limiting form of the parameters in this case can be calculated using standard asymptotic techniques (see Appendix A) and we determine that

$$a_0 \sim -4 \log \frac{(\pi - \alpha)}{2}, \qquad a_1 \sim 2, \quad \text{as} \quad \alpha \to \pi. \tag{2.11c}$$

In terms of the solution of (2.10), we have to leading order that $w \sim A v_c(\varepsilon^{-1}(\mathbf{x} - \mathbf{x}_0)) + \cdots$ which yields

$$w(\mathbf{x}; \varepsilon) \sim A\left[\log|\mathbf{x} - \mathbf{x}_0| + \frac{1}{\nu} + \varepsilon \frac{\mathbf{p} \cdot (\mathbf{x} - \mathbf{x}_0)}{|\mathbf{x} - \mathbf{x}_0|^2} + \cdots\right], \qquad \mathbf{x} \to \mathbf{x}_0. \tag{2.12}$$

A comparison between (2.9) and (2.12) provides both a local singularity behavior and a regular part for w_0. A local singularity condition on w_1 is also specified by (2.12) but not a condition on the regular part. This
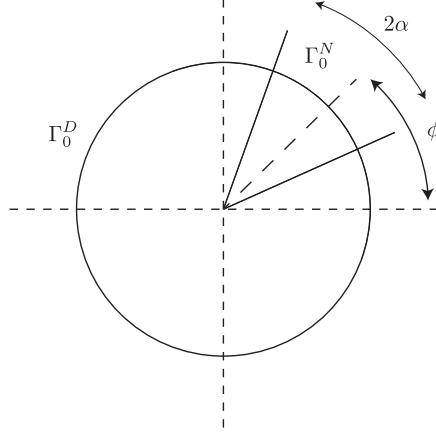
Figure 2: A unit disk trap Ω_0 which is absorbing everywhere except for a reflecting portion of arc length 2α inclined at an angle ϕ from the horizontal.

latter condition will be obtained from a higher order expansion of the inner problem. The problem for w_0 is

$$\Delta w_0 = -\frac{1}{D}, \quad \mathbf{x} \in \Omega; \qquad \frac{\partial w_0}{\partial n} = 0, \quad \mathbf{x} \in \partial\Omega; \tag{2.13a}$$

$$w_0 \sim A\left[\log|\mathbf{x} - \mathbf{x}_0| + \frac{1}{\nu} + \cdots\right], \qquad \mathbf{x} \to \mathbf{x}_0. \tag{2.13b}$$

This solution can be conveniently represented with the modified Neumann Green's function $G_m(\mathbf{x}; \boldsymbol{\xi})$ satisfying (1.3). In terms of $G_m(\mathbf{x}; \boldsymbol{\xi})$, the solution of (2.13) is written as

$$w_0 = -2\pi A G_m(\mathbf{x}; \mathbf{x}_0) + \chi_0, \tag{2.14}$$

where χ_0 is the leading order average MFPT, $\chi_0 = |\Omega|^{-1}\int_\Omega w_0\, d\mathbf{x}$, based on a uniform distribution of initial locations. The constant A is determined from a solvability condition to have value

$$A = \frac{|\Omega|}{2\pi D}, \tag{2.15}$$

while χ_0 is found by matching (2.13b) to (2.14) as $\mathbf{x} \to \mathbf{x}_0$. Taking $\mathbf{x} \to \mathbf{x}_0$ in (2.14) gives

$$w_0 \sim A\log|\mathbf{x} - \mathbf{x}_0| - 2\pi A\left[R_m(\mathbf{x}_0; \mathbf{x}_0) + \nabla_\mathbf{x} R_m \cdot (\mathbf{x} - \mathbf{x}_0) + \mathcal{O}(|\mathbf{x} - \mathbf{x}_0|^2)\right] + \chi_0. \tag{2.16}$$

The strengths of the singularities in expressions (2.16) and (2.13b) match and regular parts agree when

$$\chi_0 = \frac{|\Omega|}{D}\left[\frac{1}{2\pi\nu} + R_m(\mathbf{x}_0; \mathbf{x}_0)\right]. \tag{2.17}$$

The leading order average MFPT w_0 is now fully specified by (2.14), and the average MFPT with respect to a distribution of initial locations can be calculated.

The dependence of the MFPT on the orientation of the trap is not forthcoming in this leading order formula and so we proceed to calculate the $\varepsilon w_1(\mathbf{x}; \nu)$ term of (2.9). The local behavior of w_1 as $\mathbf{x} \to \mathbf{x}_0$ is fully specified by resolving the inner solution to $\mathcal{O}(\varepsilon)$ from which a regular part is obtained as a counterpart to the dipole singularity already established in (2.12). Writing (2.16) in terms of the variable $\mathbf{y} = \varepsilon^{-1}(\mathbf{x} - \mathbf{x}_0)$ indicates that the inner solution should be expanded to $\mathcal{O}(\varepsilon)$ as

$$v(\mathbf{y}; \varepsilon) = A\left[v_c(\mathbf{y}) - 2\pi\varepsilon\nabla_\mathbf{x} R_m(\mathbf{x}_0; \mathbf{x}_0) \cdot \mathbf{V}_c + \cdots\right],$$

where $\mathbf{V}_c$ is the vector valued function satisfying

$$\Delta\mathbf{V}_c = 0, \qquad \mathbf{y} \in \mathbb{R}^2 \setminus \Omega_0; \tag{2.18a}$$

$$\mathbf{V}_c = 0 \quad \text{on} \quad \Gamma_0^a, \qquad \frac{\partial\mathbf{V}_c}{\partial n} = 0 \quad \text{on} \quad \Gamma_0^r; \tag{2.18b}$$

$$\mathbf{V}_c(\mathbf{y}) = \mathbf{y} + \mathbf{b} + o(1), \qquad |\mathbf{y}| \to \infty, \tag{2.18c}$$

5

and $\mathbf{b}$ is a vector valued constant. The evaluation of $\mathbf{b}$ is considered in Appendix A. In the situation displayed in Fig. 2, we find that

$$\mathbf{b} = b_0 \begin{bmatrix} \cos\phi \\ \sin\phi \end{bmatrix}, \qquad b_0 = \frac{2\sqrt{2}}{\pi} \int_0^\alpha \frac{\sin u \sin\frac{u}{2}}{\sqrt{\cos u - \cos\alpha}} \, \mathrm{d}u. \tag{2.18d}$$

Returning to variables of the outer region, the local behavior of w is found to be

$$w \sim A\left[\log|\mathbf{x} - \mathbf{x}_0| + \frac{1}{\nu}\right] + \varepsilon A\left[\frac{\mathbf{p}\cdot(\mathbf{x} - \mathbf{x}_0)}{|\mathbf{x} - \mathbf{x}_0|^2} - 2\pi\nabla_\mathbf{x} R_m(\mathbf{x}_0; \mathbf{x}_0)\cdot\mathbf{b} + \mathcal{O}(1)\right].$$

This local behavior specifies the behavior of w_1 as $\mathbf{x} \to \mathbf{x}_0$, yielding the problem

$$\Delta w_1 = 0, \quad \mathbf{x} \in \Omega; \qquad \frac{\partial w_1}{\partial n} = 0, \quad \mathbf{x} \in \partial\Omega; \tag{2.19a}$$

$$w_1 \sim A\left[\frac{\mathbf{p}\cdot(\mathbf{x} - \mathbf{x}_0)}{|\mathbf{x} - \mathbf{x}_0|^2} - 2\pi\nabla_\mathbf{x} R_m(\mathbf{x}_0; \mathbf{x}_0)\cdot\mathbf{b} + \mathcal{O}(1)\right], \quad \mathbf{x} \to \mathbf{x}_0. \tag{2.19b}$$

In terms of $G_m(\mathbf{x}; \boldsymbol{\xi})$ satisfying (1.3), the solution of (2.19) is expressed as

$$w_1 = 2\pi A\, \mathbf{p}\cdot\nabla_{\boldsymbol{\xi}} G_m(\mathbf{x}; \mathbf{x}_0) + \chi_1. \tag{2.20}$$

The value of the constant χ_1 is determined by matching the local behavior of (2.20) to that specified by (2.19b), yielding that

$$\chi_1 = -2\pi A\left[\mathbf{b}\cdot\nabla_\mathbf{x} R_m(\mathbf{x}_0; \mathbf{x}_0) + \mathbf{p}\cdot\nabla_{\boldsymbol{\xi}} R_m(\mathbf{x}_0; \mathbf{x}_0)\right].$$

The symmetry property $G_m(\mathbf{x}; \mathbf{y}) = G_m(\mathbf{y}; \mathbf{x})$ of (1.3) means $\nabla_\mathbf{x} R_m(\mathbf{x}_0; \mathbf{x}_0) = \nabla_{\boldsymbol{\xi}} R_m(\mathbf{x}_0; \mathbf{x}_0)$ which yields the three term asymptotic expression for the average MFPT from a uniform distribution of starting points

$$\tau = \frac{1}{|\Omega|}\int_\Omega w\,\mathrm{d}\mathbf{x} = \chi_0 + \varepsilon\chi_1 + \cdots$$

$$\sim \frac{|\Omega|}{D}\left[\frac{1}{2\pi\nu} + R_m(\mathbf{x}_0; \mathbf{x}_0) - \varepsilon(\mathbf{p} + \mathbf{b})\cdot\nabla_\mathbf{x} R_m(\mathbf{x}_0; \mathbf{x}_0)\right]. \tag{2.21}$$

This completes the derivation of the main result (1.2).

2.1   Unit disk and comparison of MFPT with numerics

To compare the formula (1.2) directly with numerics, we consider Ω to be the unit disk, for which the modified Neumann Green's function satisfying (1.3) is known explicitly as (cf. [30])

$$G_m(\mathbf{x}; \boldsymbol{\xi}) = \frac{-1}{2\pi}\log|\mathbf{x} - \boldsymbol{\xi}| + R_m(\mathbf{x}; \boldsymbol{\xi}),$$

$$R_m(\mathbf{x}; \boldsymbol{\xi}) = \frac{-1}{2\pi}\left(\log\left|\mathbf{x}|\boldsymbol{\xi}| - \frac{\boldsymbol{\xi}}{|\boldsymbol{\xi}|}\right| - \frac{1}{2}(|\mathbf{x}|^2 + |\boldsymbol{\xi}|^2) + \frac{3}{4}\right). \tag{2.22a}$$

The gradient of the regular part $R_m(\mathbf{x}; \boldsymbol{\xi})$ is computed to be

$$\nabla_\mathbf{x} R_m(\mathbf{x}; \boldsymbol{\xi}) = \frac{-1}{2\pi}\left(\frac{\mathbf{x}|\boldsymbol{\xi}|^2 - \boldsymbol{\xi}}{\left|\mathbf{x}|\boldsymbol{\xi}| - \frac{\boldsymbol{\xi}}{|\boldsymbol{\xi}|}\right|^2} - \mathbf{x}\right). \tag{2.22b}$$

Assuming that the trap lies on the x-axis, $\boldsymbol{\xi} = (r_0, 0)$, we then obtain

$$R_m(\boldsymbol{\xi}; \boldsymbol{\xi}) = \frac{-1}{2\pi}\left[\log(1 - r_0^2) - r_0^2 + \frac{3}{4}\right], \qquad \nabla_\mathbf{x} R_m(\boldsymbol{\xi}; \boldsymbol{\xi}) = \frac{1}{2\pi}\left(\frac{r_0(2 - r_0^2)}{1 - r_0^2}, 0\right), \tag{2.22c}$$
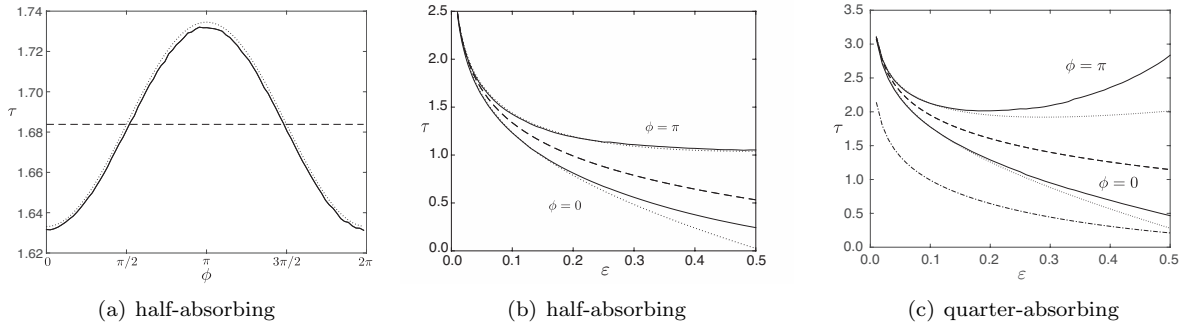
6

(a) half-absorbing (b) half-absorbing (c) quarter-absorbing

Figure 3: Example with one trap centered at $\mathbf{x}_0 = (0.45, 0)$. In (a), we compare the asymptotic result (2.23) for τ versus ϕ (dotted line) against the numerical result (solid line) with a half-absorbing trap. Here, $\varepsilon = 0.05$. In (b) and (c), we show a comparison of MFPT between the leading order expression (2.17) (dashed line), high order expansion (2.23) (dotted line), together with full numerics (solid line). The high order expansion agrees very well with the numerical solution, even when ε is moderately large. Note, the leading order term does not include orientation information and does not change with ϕ. In (c), we provide τ for a fully absorbing trap for reference (dashed-dotted). Note that, unlike the $\phi = \pi$ case, it decreases monotonically with ε.

and
$$\tau = \frac{1}{2D} \left[\log \frac{1}{\varepsilon d_0} - \left(\log(1 - r_0^2) - r_0^2 + \frac{3}{4} \right) - \varepsilon(a_1 + b_0) \frac{r_0(2 - r_0^2)}{1 - r_0^2} \cos \phi \right], \tag{2.23}$$

where ϕ denotes the orientation of the reflecting portion of the trap.

In Fig. 3(a), this formula is compared with direct numerical computation of τ by solving the PDE (1.1) using Matlab's PDE solver. We observe that, in agreement with (2.23), the MFPT is minimized when $\phi = 0$; that is, when the reflecting (absorbing) segment is oriented towards the boundary (center). In Figs. 3(b) and 3(c), we plot τ versus ε for two different orientations. We show that, even though the leading order expression term in (2.23) gives a reasonable estimate (dashed line), especially for small ε, it does not distinguish between different orientations of the trap. The effect of orientation is secondary to that of the size of the trap, and is captured by the higher order term in (2.23). As such, agreement between the high-order asymptotic result and the numerical result persists for a larger range of ε. Note, however, that the asymptotics begin to break down when ε becomes too large. In particular, for a trap centered $\mathbf{x}_0 = (0.45, 0)$ with a quarter absorbing window facing the boundary, we observe in Fig. 3(b) a "shielding effect" whereby for ε sufficiently large, placing the window very close to the boundary causes τ to increase when $\varepsilon > 0.2$. This illustrates an important consequence of a trap with a mixed configuration of absorbing and reflecting sections in contrast to one that is fully absorbing. For certain distributions and orientations of absorbing windows, a larger trap is in fact *detrimental* to reducing mean capture times. The physical interpretation is that the absorbing portion of the trap can be obstructed or shielded from the majority of the domain if it is close to, and aligned towards, the boundary, therefore making it difficult to access from many initial starting points. Therefore, a quick capture time can only be achieved from a small set of initial points between the trap and the boundary. This phenomenon is entirely absent for a fully absorbing trap, where MFPT decreases monotonically with trap size.

3 An asymptotic formula for Laplacian eigenvalue

In this section, we obtain the asymptotic formula (1.8) for the fundamental eigenfunction and eigenvalue of problem (1.4) in the limit as $\varepsilon \to 0$. In the vicinity of $\mathbf{x}_0$, the rescaled variables

$$\mathbf{y} = \frac{\mathbf{x} - \mathbf{x}_0}{\varepsilon}, \qquad u(\mathbf{x}_0 + \varepsilon \mathbf{y}) = v(\mathbf{y}) \tag{3.24}$$

7

are introduced and $v(\mathbf{y})$ is expanded as

$$v(\mathbf{y}) = v_0(\mathbf{y}) + \mu(\varepsilon)v_1(\mathbf{y}) + \cdots, \tag{3.25}$$

where $\mu(\varepsilon)$ is a gauge function to be determined. The leading order problem is written as $v_0 = A(\nu)v_c(\mathbf{y})$ where $v_c(\mathbf{y})$ is a canonical harmonic function with mixed boundary conditions specified in (2.10). The far field behavior of (2.10c) expressed in terms of the original variables (3.24) motivates the expansion

$$u = u_0(\mathbf{x};\nu) + \varepsilon u_1(\mathbf{x};\nu) + \cdots, \qquad \lambda = \lambda_0(\nu) + \varepsilon\lambda_1(\nu) + \cdots \qquad \nu(\varepsilon) = \frac{-1}{\log \varepsilon d_0}. \tag{3.26}$$

The equations for the terms in (3.26) are supplemented with the local behavior as $\mathbf{x} \to \mathbf{x}_0$

$$u \sim A(\nu)v_c\left(\frac{\mathbf{x} - \mathbf{x}_0}{\varepsilon}\right) \sim A \log |\mathbf{x} - \mathbf{x}_0| + \frac{A}{\nu} + \varepsilon A\frac{\mathbf{p} \cdot (\mathbf{x} - \mathbf{x}_0)}{|\mathbf{x} - \mathbf{x}_0|^2}, \qquad \mathbf{x} \to \mathbf{x}_0. \tag{3.27}$$

Here, $A = A(\nu)$ is a normalization constant with dependence on $\nu = -1/\log(\varepsilon d_0)$. This singularity behavior augments the equations for u_0 and u_1 which allows the determination of λ_0 and λ_1. At leading order, u_0 satisfies

$$\Delta u_0 + \lambda_0 u_0 = 0, \qquad \mathbf{x} \in \Omega \setminus \{\mathbf{x}_0\}; \qquad \frac{\partial u_0}{\partial n} = 0, \quad \mathbf{x} \in \partial\Omega; \tag{3.28a}$$

$$\int_\Omega u_0^2 \, d\mathbf{x} = 1; \qquad u_0 \sim A \log |\mathbf{x} - \mathbf{x}_0| + \frac{A}{\nu} + o(1), \qquad \mathbf{x} \to \mathbf{x}_0. \tag{3.28b}$$

The singularity behavior (3.28b) prescribes both the strength of the singularity and a regular part as $\mathbf{x} \to \mathbf{x}_0$. A convenient representation of the solution to (3.28) is available in terms of the Helmholtz Green's function $G_h(\mathbf{x};\boldsymbol{\xi},\lambda)$, and its regular part $R_h(\mathbf{x};\boldsymbol{\xi},\lambda)$ satisfying (1.7). This Green's function can be utilized to represent the solution of (3.28) in the form $u_0 = -2\pi A G_h(\mathbf{x};\mathbf{x}_0,\lambda_0)$. The constant A will later be specified by the normalization condition $\langle u_0, u_0 \rangle = 1$. The local behavior of u_0 as $\mathbf{x} \to \mathbf{x}_0$ may now be expressed as

$$u_0 \sim A\big(\log |\mathbf{x} - \mathbf{x}_0| - 2\pi R_{h0} - 2\pi(\mathbf{x} - \mathbf{x}_0) \cdot \nabla R_{h0} + \cdots \big), \qquad \mathbf{x} \to \mathbf{x}_0, \tag{3.29}$$

where

$$R_{h0} = R_h(\mathbf{x}_0;\mathbf{x}_0,\lambda_0), \qquad \nabla R_{h0} = \nabla_{\mathbf{x}} R_h(\mathbf{x};\mathbf{x}_0,\lambda_0)\Big|_{\mathbf{x}=\mathbf{x}_0}. \tag{3.30}$$

The strength of the singularity corresponds to that prescribed by (3.28b), while matching the regular part of (3.29) to (3.28b) yields the transcendental equation

$$R_{h0} = R_h(\mathbf{x}_0;\mathbf{x}_0,\lambda_0(\nu)) = \frac{-1}{2\pi\nu}, \qquad \nu = \frac{-1}{\log \varepsilon d_0}. \tag{3.31}$$

Equation (3.31) determines a $\lambda_0(\nu)$ which "sums the logs" and is accurate beyond any order ν^M for integer M. For a few cases in which $R_h(\mathbf{x}_0;\mathbf{x}_0,\lambda_0)$ can be computed explicitly, such as $\Omega = \{|\mathbf{x}| \le 1\}$, equation (3.31) may be simplified. In general, this equation must be solved numerically from simulation of the full PDE (1.7).

The dependence of the leading order eigenvalue λ_0 on the particular characteristics of the hole configuration is encapsulated in the product εd_0. The configuration of the absorbing and reflecting sections of the trap (i.e., where they are distributed relative to each other) determines the value of d_0. However, information regarding the orientation of the trap is absent. We now look to obtain the correction term which incorporates the dipole vector of the trap and alignment information regarding the absorbing and reflecting sections. The equation for (u_1, λ_1) is

$$\Delta u_1 + \lambda_0 u_1 = -\lambda_1 u_0, \quad \mathbf{x} \in \Omega; \qquad \frac{\partial u_1}{\partial n} = 0 \quad \mathbf{x} \in \partial\Omega; \tag{3.32a}$$

$$\int_\Omega u_0 u_1 \, d\mathbf{x} = 0, \qquad u_1 \sim \text{singular}, \qquad \mathbf{x} \to \mathbf{x}_0. \tag{3.32b}$$

8

To determine the full singularity behavior of u_1, it is necessary to determine the correction term $\mu(\varepsilon)v_1$ to the expansion of the inner problem (3.25). Substituting $\mathbf{x} - \mathbf{x}_0 = \varepsilon\mathbf{y}$ into the local behavior (3.29) yields that $\mu(\varepsilon) = \varepsilon$ and that v_1 admits the representation

$$v_1(\mathbf{y}) = A\Big[Cv_c - 2\pi\,\nabla R_{h0} \cdot \mathbf{V}_c\Big], \tag{3.33}$$

where C is a constant and $\mathbf{V}_c$ satisfies the vector valued problem (2.18). Reconstituting the far field behavior for the outer problem gives

$$
\begin{aligned}
u \sim{}& v_0\Big(\frac{\mathbf{x}-\mathbf{x}_0}{\varepsilon}\Big) + \varepsilon v_1\Big(\frac{\mathbf{x}-\mathbf{x}_0}{\varepsilon}\Big) + \cdots \\
\sim{}& A\Big[\log|\mathbf{x}-\mathbf{x}_0| + \frac{1}{\nu} - 2\pi\nabla R_{h0}\cdot(\mathbf{x}-\mathbf{x}_0)\Big] \\
&+ \varepsilon A\Big[\frac{\mathbf{p}\cdot(\mathbf{x}-\mathbf{x}_0)}{|\mathbf{x}-\mathbf{x}_0|^2} + C\log|\mathbf{x}-\mathbf{x}_0| + \frac{C}{\nu} - 2\pi\nabla R_{h0}\cdot\mathbf{b}\Big] + \cdots.
\end{aligned}
$$

This singularity behavior cannot be matched to the outer solution unless C is chosen as

$$C = 2\pi\nu\nabla R_{h0}\cdot\mathbf{b}, \tag{3.34}$$

which results in the following full problem for u_1

$$\Delta u_1 + \lambda_0 u_1 = -\lambda_1 u_0, \quad \mathbf{x}\in\Omega; \qquad \frac{\partial u_1}{\partial n} = 0 \quad \mathbf{x}\in\partial\Omega; \qquad \int_\Omega u_0 u_1\,d\mathbf{x} = 0, \tag{3.35a}$$

$$u_1 \sim A\frac{\mathbf{p}\cdot(\mathbf{x}-\mathbf{x}_0)}{|\mathbf{x}-\mathbf{x}_0|^2} + 2\pi A\nu(\nabla R_{h0}\cdot\mathbf{b})\log|\mathbf{x}-\mathbf{x}_0| + \mathcal{O}(1), \qquad \mathbf{x}\to\mathbf{x}_0. \tag{3.35b}$$

To incorporate the singularity structure of (3.35b) into a solvability condition determining λ_1, we multiply (3.35a) by u_0 and integrate over $\Omega\setminus B(\mathbf{x}_0,\sigma)$, where $B(\mathbf{x}_0,\sigma)$ is a ball of radius σ centered at $\mathbf{x}_0$ and pass to the limit $\sigma\to 0$. Beginning with Green's second identity we have,

$$
\begin{aligned}
\lambda_1\int_{\Omega\setminus B(\mathbf{x}_0,\sigma)} u_0^2\,d\mathbf{x} &= \int_{\Omega\setminus B(\mathbf{x}_0,\sigma)} u_1(\Delta u_0 + \lambda_0 u_0) - u_0(\Delta u_1 + \lambda_0 u_1)\,d\mathbf{x} \\
&= \int_{|\mathbf{x}-\mathbf{x}_0|=\sigma} u_1\partial_n u_0 - u_0\partial_n u_1\,ds.
\end{aligned}
\tag{3.36a}
$$

We now move to a polar coordinate system $(\mathbf{x}-\mathbf{x}_0) = r(\cos\theta,\sin\theta) = r\,\mathbf{e}$ for $\mathbf{e} = (\cos\theta,\sin\theta)$ in which $\partial_n = -\partial_r$ and the local behavior of u_0 and u_1 as $r\to 0$ is given by

$$u_0 \sim A\log r - 2\pi A\big(R_{h0} + r\mathbf{e}\cdot\nabla R_{h0} + \cdots\big), \qquad \partial_r u_0 \sim \frac{A}{r} - 2\pi A\mathbf{e}\cdot\nabla R_{h0} + \cdots$$

$$u_1 \sim A\frac{\mathbf{p}\cdot\mathbf{e}}{r} + 2\pi A\nu(\nabla R_{h0}\cdot\mathbf{b})\log r + \cdots, \qquad \partial_r u_1 \sim -A\frac{\mathbf{p}\cdot\mathbf{e}}{r^2} + 2\pi A\nu\frac{\nabla R_{h0}\cdot\mathbf{b}}{r} + \cdots.$$

Substituting this into (3.36) and passing to the limit $\sigma\to 0$, we have that

$$
\begin{aligned}
\lambda_1\langle u_0, u_0\rangle &= -\lim_{\sigma\to 0}\int_0^{2\pi} \sigma A^2\left[\Big(\frac{\mathbf{p}\cdot\mathbf{e}}{\sigma} + 2\pi\nu(\nabla R_{h0}\cdot\mathbf{b})\log\sigma\Big)\Big(\frac{1}{\sigma} - 2\pi\,\mathbf{e}\cdot\nabla R_{h0}\Big)\right. \\
&\qquad\left. -\Big(\log\sigma - 2\pi(R_{h0} + \sigma\mathbf{e}\cdot\nabla R_{h0})\Big)\Big(-\frac{\mathbf{p}\cdot\mathbf{e}}{\sigma^2} + 2\pi\nu\frac{\nabla R_{h0}\cdot\mathbf{b}}{\sigma}\Big)\right]\,d\theta \\
&= 4\pi A^2\int_0^{2\pi} [(\mathbf{p}\cdot\mathbf{e})(\mathbf{e}\cdot\nabla R_{h0}) - 4\pi^2\nu R_{h0}\nabla R_{h0}\cdot\mathbf{b}]\,d\theta \\
&= 4\pi^2 A^2\Big(\mathbf{p} - 2\pi\nu R_{h0}\,\mathbf{b}\Big)\cdot\nabla R_{h0}. \tag{3.37}
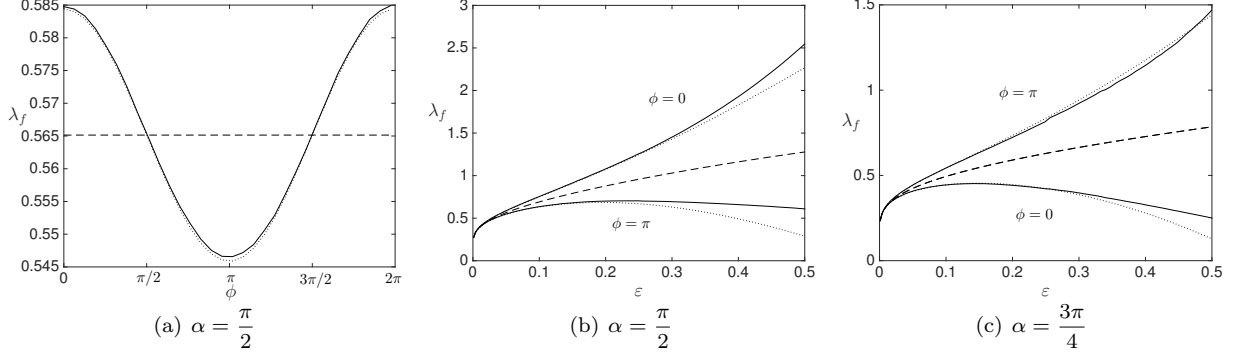\end{aligned}
$$

Figure 4: (a) Plot of the fundamental eigenvalue λ_f of (1.4) against trap orientation angle ϕ for $\mathbf{x}_0 = (0.45, 0)$, $\varepsilon = 0.05$ and $\alpha = \pi/2$. (b) Plot of λ_f vs. ε with ϕ as indicated and $\alpha = \pi/2$. (c) Same as (b) except with $\alpha = 3\pi/4$. In above figures, solid curve is full numerical simulations of (1.4), dashed curve is leading order term asymptotic formula (3.31), dotted curve is two term asymptotic formula (3.38).

The constant A is determined by the normalization condition $\langle u_0, u_0 \rangle = 1$ to satisfy $4\pi^2 A^2 \langle G_h, G_h \rangle = 1$ while using $2\pi\nu R_{h0} = -1$ from (3.31) yields the final result

$$\lambda_f = \lambda_0 + \varepsilon\lambda_1 + \cdots, \qquad \lambda_1 = \frac{(\mathbf{p} + \mathbf{b}) \cdot \nabla R_{h0}}{\langle G_h, G_h \rangle}, \tag{3.38}$$

where $\lambda_0(\nu)$ is determined from equation (3.31) and G_h solves (1.7).

3.1 Comparison with numerics for λ_f

We now compare the asymptotic result (3.38) for the fundamental Laplacian eigenvalue of (1.4) on the unit disk and with a circular trap centered at $\mathbf{x}_0$.

Example 1 - Half absorbing, half reflecting trap. In this example, we take $\mathbf{x}_0 = (0.45, 0)$ with $\alpha = \pi/2$ so that $|\Gamma_0^r|/|\Gamma_0^a| = 1$ (refer to Fig. 2). For this special value of α, we obtain (see Appendix A, equations (A.18) and (A.19)),

$$d_0 = \frac{1}{2}, \quad \mathbf{p} = a_1(\cos\phi, \sin\phi), \quad a_1 = 1, \qquad \mathbf{b} = b_0(\cos\phi, \sin\phi), \quad b_0 = 1.$$

When $\varepsilon = 0.05$, the leading order eigenvalue is found from numerical simulation of (3.31) to be $\lambda_0 \sim 0.5651$. We also numerically calculate the term

$$\frac{\nabla R_{h0}}{\langle G_h, G_h \rangle} = (0.1926, 0.0000). \tag{3.39}$$

In Fig. 4(a), we see good agreement between the full numerical solution and the reduced asymptotic formula (3.38). For a fixed ε, the maximum of λ_f occurs when $\phi = 0$ corresponding to the reflecting portion facing towards the boundary (i.e. the absorbing portion facing towards the center). The minimum of λ_f occurs for $\phi = \pi$ when the reflecting portion is orientated towards the center of the domain (i.e. the absorbing portion is facing towards the boundary). As expected from the inverse relation between the fundamental eigenvalue and MFPT (see (1.5) and (1.6)), λ_f is maximized where τ in Fig. 3(a) is minimized.

Fig. 4(b) shows that a good agreement persists for a range of ε. For the $\phi = \pi$ case, unlike in Fig. 3(b) with the same value of α, we observe a very strong shielding effect evidenced by the clear maximum of λ_f at $\varepsilon \approx 0.2$. The difference in behavior is due to the loss in correspondence between MFPT and the fundamental eigenvalue as ε increases. The shielding effect is also observed in Fig. 4(c) for a quarter-absorbing trap and $\phi = \pi$. This effect is also observed in the corresponding plot for τ in Fig. 3(c).

Example 2 - One quarter absorbing trap. In Fig. 4(c) we take $\alpha = 3\pi/4$ corresponding to a quarter-absorbing trap and three-quarters reflecting boundary, with $\mathbf{x}_0 = (0.45, 0)$. Again, excellent agreement

10

between numerics and asymptotics is observed. The shielding effect when $\phi = \pi$ is again observed as λ_f achieves a maximum at $\varepsilon \approx 0.1$ (well approximated by asymptotics). We suspect that this is a result of the same effect that gave rise to the minimum in MFPT near $\varepsilon \approx 0.2$ for the $\phi = \pi$ case in Fig. 3(b).
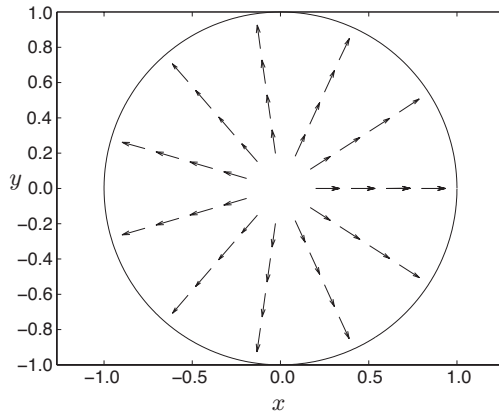

Figure 5: The normalized gradient vector ∇R_{h0} plotted at a range of points in the disk.

More generally, we note that at a fixed value of ε, the high order asymptotic formula (3.38) informs on the optimal trap orientation in terms of a geometric condition related to the gradient of the regular part of a Green's function. Writing $\mathbf{p} = a_1 \mathbf{e}$ and $\mathbf{b} = b_0 \mathbf{e}$ where $\mathbf{e} = (\cos\phi, \sin\phi)$, a simple calculation shows the optimizing trap orientations are determined by the solutions of

$$\mathbf{e} \cdot \nabla R_{h0}^{\perp} = 0. \tag{3.40}$$

The fundamental eigenvalue λ_f is therefore optimized by aligning the Neumann portion of the trap along the gradient of the regular part of the Green's function. For the case of a disk, we see in Fig. 5 that the gradient is aligned radially outwards, and therefore the eigenvalue is maximized (minimized) by aligning the Neumann portion of the trap towards (away from) the boundary in agreement with Fig. 4.

4 Trap fragmentation and prescribed motion of trap

In this section, we numerically investigate two additional facets of traps with mixed configurations of absorbing windows on MFTP. First, we consider the effects of fragmentation of the trap's absorbing section on the MFPT and in a particular case, identify a homogenized problem in the limit of large number of absorbing windows with fixed overall absorbing fraction. Second, we consider the effects on the MFPT when a mixed configuration trap undergoes prescribed motion in the domain.

4.1 Fragmentation of absorbing trap segments

In this section, we consider the scenario of a single trap Ω_0 which is reflecting everywhere apart from $N \geq 1$ non-overlapping absorbing windows along which Dirichlet boundary conditions are applied. The total absorbing fraction of the trap boundary ℓ is held fixed. In the case where each of the N traps have common arc length σ, then $\sigma N = |\partial\Omega_0|/\ell$. The distribution of the windows contributes to leading order formula for the MFPT (1.2) (also cf. [16]),

$$\tau \sim -\frac{|\Omega|}{2\pi D} \log \varepsilon d_0 + \cdots, \qquad d_0 = \exp\left[\frac{-a_0}{2}\right],$$

in the limit as $\varepsilon \to 0$, through the parameters d_0 and a_0. It is clear that configurations of windows which generate lower values of a_0 result in a reduced average MFPT. For example the fully absorbing case corresponds to the values $a_0 = 0$ and $d_0 = 1$. The main aim of this section is to study how the parameter a_0, determined from the inner problem (2.10), depends on the distribution of the windows along the boundary of the trap.

11

The main analysis of this problem is performed in the limit of small patch size $\sigma \to 0$. For the canonical inner problem $v_c(\mathbf{y})$ satisfying (2.10), we assume N absorbing windows centered at $\{\mathbf{y}_j\}_{j=1}^N \in \partial\Omega_0$ with common arc length σ. In the vicinity of each window a local problem can be formed in a arc-length tangent coordinate system and solved to obtain an effective local condition on $v_c(\mathbf{y})$ at each window. The steps of this calculation are well known and laid out in detail in §2 of [16].

The result of this analysis is that in the limit as $\sigma \to 0$, each absorbing arc is represented by a logarithmic singularity with an associated regular part. The limiting form of (2.10) consequently becomes

$$\Delta v_c = 0, \qquad \mathbf{y} \in \mathbb{R}^2 \setminus \Omega_0; \qquad \frac{\partial v_c}{\partial n} = 0, \quad \text{on} \quad \partial\Omega_0 \setminus \{\mathbf{y}_j\}_{j=1}^N; \tag{4.41a}$$

$$v_c \sim A_j \log |\mathbf{y} - \mathbf{y}_j| + \frac{A_j}{\mu} + \cdots, \qquad \mathbf{y} \to \mathbf{y}_j; \qquad j = 1, \ldots, N, \qquad \mu = \frac{-1}{\log \frac{\sigma}{4}}; \tag{4.41b}$$

$$v_c(\mathbf{y}) = \log |\mathbf{y}| - \log d_0 + \mathcal{O}\Big(\frac{1}{|\mathbf{y}|}\Big), \qquad |\mathbf{y}| \to \infty, \tag{4.41c}$$

where $\{A_j\}_{j=1}^N$ are unknown constants to be determined. The main aim is to calculate the logarithmic capacitance $\log d_0$ in the far field behavior (4.41c). In terms of a surface Green's function $G_s(\mathbf{y}; \boldsymbol{\xi})$, the solution of (4.41)

$$v_c(\mathbf{y}) = -\pi \sum_{j=1}^N A_j G_s(\mathbf{y}; \mathbf{y}_j) + \frac{a_0}{2}, \tag{4.42}$$

where a_0 is the same constant appearing in (4.50) and $G_s(\mathbf{y}; \boldsymbol{\xi})$ satisfies the exterior problem

$$\Delta G_s = 0, \quad \mathbf{y} \in \mathbb{R}^2 \setminus \Omega_0; \qquad \frac{\partial G_s}{\partial n} = 0, \quad \mathbf{y} \in \partial\Omega_0 \setminus \{\boldsymbol{\xi}\}; \tag{4.43a}$$

$$G_s(\mathbf{y}; \boldsymbol{\xi}) = \frac{-1}{\pi} \log |\mathbf{y} - \boldsymbol{\xi}| + R_s(\mathbf{y}; \boldsymbol{\xi}); \qquad \int_{\partial\Omega_0} G_s \, ds = 0; \tag{4.43b}$$

$$G_s(\mathbf{y}; \boldsymbol{\xi}) \sim \frac{-1}{2\pi} \log |\mathbf{y}| + \cdots \qquad |\mathbf{y}| \to \infty. \tag{4.43c}$$

Applying the conditions (4.41b) and (4.41c) to (4.42) gives the system of $(N+1)$ linear equations

$$\sum_{j=1}^N A_j = 2; \qquad A_k + \pi\mu\Big[A_k R_s(\mathbf{y}_k; \mathbf{y}_k) + \sum_{\substack{j=1 \\ j \neq k}}^N A_j G_s(\mathbf{y}_k; \mathbf{y}_j)\Big] = \frac{a_0\mu}{2}, \qquad k = 1, \ldots, N. \tag{4.44}$$

A more compact representation of the linear system (4.44) in matrix form is

$$\big[I + \pi\mu\mathcal{G}\big]\mathbf{A} = \frac{a_0\mu}{2}\mathbf{e}; \qquad \mathbf{e}^T\mathbf{A} = 2, \tag{4.45a}$$

where I is the $N \times N$ identity matrix and

$$\mathcal{G}_{ij} = \begin{cases} R_s(\mathbf{x}_i; \mathbf{x}_i) & i = j \\ G_s(\mathbf{x}_i; \mathbf{x}_j) & i \neq j \end{cases} \qquad \begin{matrix} \mathbf{A}_j = A_j, \\ \mathbf{e}_j = 1, \end{matrix} \qquad j = 1, \ldots, N. \tag{4.45b}$$

In the limit $\mu \to 0$, the asymptotic inverse $[I + \pi\mu\mathcal{G}]^{-1} \sim [I - \pi\mu\mathcal{G}]$ can be applied to obtain

$$a_0 = \frac{4}{\mu N} + \frac{4\pi}{N^2}\mathbf{e}^T\mathcal{G}\mathbf{e} = \frac{4}{\mu N} + \frac{4\pi}{N^2}\sum_{i=1}^N\sum_{j=1}^N \mathcal{G}_{ij} + \mathcal{O}(\mu); \qquad \mu = \frac{-1}{\log \frac{\sigma}{4}}. \tag{4.46}$$

A comparison with (4.41c) provides the relationship $a_0/2 = -\log d_0$ for a_0 and so (4.46) is an analytic expression for effective logarithmic capacitance for N well-separated small absorbing windows.

For a detailed quantitative comparison, we specialize to the case where Ω_0 is the unit disc and the N absorbing windows are centered at the roots of unity. In this case, we calculate that

$$G_s(\mathbf{y}; \boldsymbol{\xi}) = \frac{-1}{\pi} \log |\mathbf{y} - \boldsymbol{\xi}| + \frac{1}{2\pi} \log |\mathbf{y}|, \tag{4.47}$$
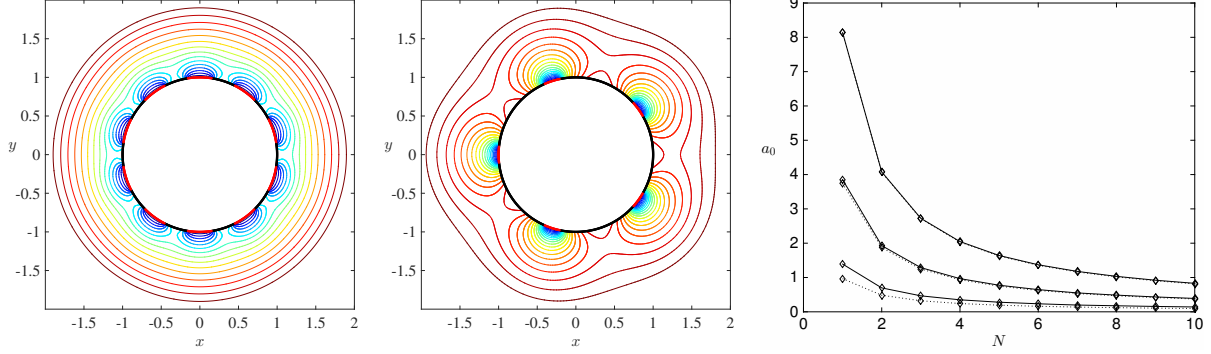
Figure 6: Left and middle: iso-potentials of solution to (2.10) with black indicating reflecting sections and red indicating absorbing. Left: half absorbing and half reflecting with $N = 10$ absorbing patches. Middle: $N = 5$ with total absorbing fraction $\ell = \frac{1}{6}$. Right: Subdivision of the absorbing section into N windows centered at the roots of unity. The curves a_0 against N are plotted for traps with absorbing fractions $\ell = \frac{1}{12}, \frac{1}{4}, \frac{1}{2}$. Full numerical (solid) curve agrees closely with asymptotic (dashed) prediction formula (4.49).

which simplifies (4.46) to

$$a_0 = \frac{4}{\mu N} - \frac{4}{N^2} \sum_{i=1}^{N} \log \prod_{\substack{j=1 \\ j \neq i}}^{N} |\mathbf{y}_i - \mathbf{y}_j|. \tag{4.48}$$

Note, in this case, that the self-interaction terms $R_s(\mathbf{y}_k; \mathbf{y}_k)$ in (4.44) are zero. If the centers of the absorbing windows are distributed periodically at locations $\mathbf{y}_j = (\cos \frac{2\pi j}{N}, \sin \frac{2\pi j}{N})$ for $j = 1, \ldots, N$, expression (4.48) simplifies further to

$$a_0 = \frac{4}{\mu N} - \frac{4}{N^2}(N \log N) = -\frac{4}{N} \log \left(\frac{\sigma N}{4} \right). \tag{4.49}$$

This closed form expression (4.49) for the logarithmic capacitance confirms that $a_0 \to 0$ for fixed $\sigma N = 2\pi\ell$ and $N \to \infty$, in agreement with numerical simulation of (4.50). In the case $N = 1$ and $\pi\ell = \pi - \alpha$, expression (4.49) agrees with (2.11c) which is derived from the exact result (2.11a) for a_0 in the limit of of one small absorbing segment. Therefore, subdivision of absorbing windows results in a reduced MFPT and in the limit $N \to \infty$, the MFPT approaches that generated by a fully absorbing trap, even though the absorbing fraction ℓ is asymptotically small.

In the case where Ω_0 is a disc, a separable solution for $v_c(\mathbf{y})$ can be formulated (cf. Appendix (A.1)-(A.4)) in polar coordinates which gives rise to the dual trigonometric series

$$\begin{cases} \dfrac{a_0}{2} + \displaystyle\sum_{n=1}^{\infty} a_n \cos n\theta = 0, & \text{on absorbing sections;} \\ \displaystyle\sum_{n=1}^{\infty} n a_n \cos n\theta = 1, & \text{on reflecting sections.} \end{cases} \tag{4.50}$$

To validate the asymptotic formula (4.49), we formulate a numerical solution of (4.50) by truncating the series at $M = 2500$ modes and constructing a linear system for the unknowns $\{a_n\}_{n=0}^{M}$ by evaluating (4.50) at a range of values of θ. In Fig. 6, a_0 is plotted as a function of the number of subdivisions N. The fragmentation of the traps decreases a_0 and gives the limiting behavior $a_0 \to 0$ as $N \to \infty$. As an all absorbing trap corresponds to $a_0 = 0$ and $d_0 = 1$, fragmentation of the absorbing and reflecting portions can be understood to increase the capturing capacity of the trap. The asymptotic formula (4.49) and full numerical solutions of $a_0(N)$ from (4.50) agree very closely as $N \to \infty$ and $\sigma \to 0$ for σN fixed.

13

	$N = 1$	$N = 2$	$N = 4$	$N = 8$	$N = 16$
$\ell = \frac{1}{2}$	0.0910	0.0442	0.0227	0.0113	0.0057
$\ell = \frac{1}{3}$	0.0526	0.0146	0.0074	0.0037	0.0018
$\ell = \frac{1}{4}$	0.0416	0.0047	0.0023	0.0010	0.0005

Table 1: Values of $|\tau - \tau_h|$ for a single circular trap of radius $\varepsilon = 0.05$ centered at $\mathbf{x}_0 = (0.25, 0)$ with N absorbing windows of common arc length and cumulative arc length $2\pi\ell$. Values of τ and τ_h are determined from numerical simulation of (1.1) and (4.52).

4.1.1 Homogenization Limit

We now identify a homogenized problem for a periodic arrangement of absorbing windows in the limit as $\sigma \to 0$ and $N \to \infty$ with fixed total absorbing length $\sigma N = 2\pi\ell$. In the dilute fraction limit $\ell \ll 1$, the mixed configuration of Neumann and Dirichlet boundary conditions can be replaced by an effective Robin condition to arrive at a homogenized problem v_h satisfying

$$\Delta v_h = 0, \quad |\mathbf{y}| > 1; \qquad \sigma \frac{\partial v_h}{\partial n} + \kappa(\ell)\, v_h = 0, \quad |\mathbf{y}| = 1; \tag{4.51a}$$

$$v_h(\mathbf{y}) = \log|\mathbf{y}| - \log d_h + \mathcal{O}\Big(\frac{1}{|\mathbf{y}|}\Big), \qquad |\mathbf{y}| \to \infty, \tag{4.51b}$$

where, from matching the logarithmic capacitance to (4.49), the parameters

$$\kappa(\ell) = \frac{-\pi\ell}{\log \frac{\pi\ell}{2}}, \qquad d_h = \Big(\frac{\pi\ell}{2}\Big)^{\frac{2}{N}}, \tag{4.51c}$$

are obtained. The solution of $v_h(\mathbf{y})$ constitutes the profile in a $\mathcal{O}(\varepsilon)$ vicinity of the trap, which gives rise to a homogenized problem w_h for the mean first passage (1.1)

$$D\Delta w_h + 1 = 0, \quad \mathbf{x} \in \Omega \setminus \Omega_\varepsilon; \qquad \frac{\partial w_h}{\partial n} = 0, \quad \mathbf{x} \in \partial\Omega; \tag{4.52a}$$

$$\varepsilon\, \sigma \frac{\partial w_h}{\partial n} + \kappa(\ell)\, w_h = 0, \qquad \mathbf{x} \in \partial\Omega_\varepsilon, \tag{4.52b}$$

where $\Omega_\varepsilon = \{\mathbf{x} \in \mathbb{R}^2 \mid |\mathbf{x} - \mathbf{x}_0| < \varepsilon\}$. The average MFPT from a uniform distribution of starting locations is $\tau_h = |\Omega|^{-1} \int_\Omega w_h(\mathbf{x})\, d\mathbf{x}$. In Table 1, the convergence of τ_h to τ as $N \to \infty$ with fixed σN is verified. These two quantities are in close agreement when $\sigma = 2\pi\ell/N$ is small as in this regime, the validity of the asymptotic formulation for the logarithmic capacitance (4.49) is strongest. As the homogenized inner problem (4.51) is radially symmetric, an important conclusion of this analysis is that in the large N limit, the total absorbing fraction ℓ is the main indicator of the capturing effectiveness of the trap, and orientation is largely irrelevant.

4.2 Rotating trap

Next, we investigate numerically the effect of rotation on the mixed single trap. This scenario was recently investigated for an entirely absorbing trap in [31]. For a trap with center $\mathbf{x}_0 = r_0(\cos\omega t, \sin\omega t)$ with $r_0 = |\mathbf{x}_0|$, we move to a frame in which the trap is stationary with the transformation $\mathbf{x} \to e^{i\omega t}\mathbf{x}$, which gives rise to the problem for the MFPT $w(\mathbf{x}; \omega)$

$$D\Delta w + \omega w_\theta + 1 = 0, \qquad \mathbf{x} \in \Omega; \tag{4.53a}$$

$$\frac{\partial w}{\partial n} = 0, \quad \text{on} \quad \partial\Omega; \tag{4.53b}$$

$$w = 0, \quad \text{on} \quad \Gamma_\varepsilon^a, \qquad \frac{\partial w}{\partial n} = 0 \quad \text{on} \quad \Gamma_\varepsilon^r. \tag{4.53c}$$
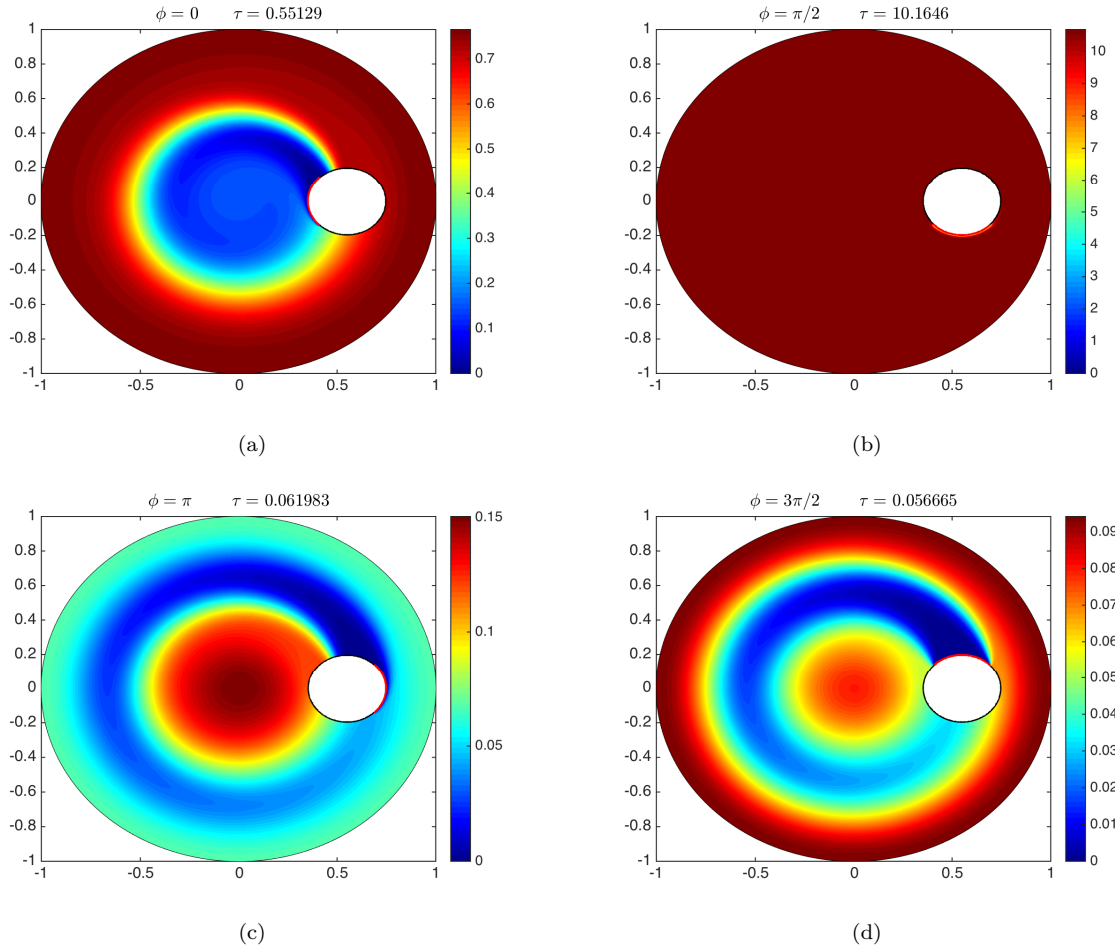
14

Figure 7: MFPT for a trap rotating clockwise with large angular velocity $\omega = 500$. In the moving frame, the trap is centered at $\mathbf{x}_0 = (0.55, 0)$ with radius is $\varepsilon = 0.2$. For a very fast angular velocity, trap orientation determines the leading-order MFPT behavior.

For a more detailed derivation of (4.53) see [31].

Figure 7 shows the dramatic effect that the rotation can have on MFPT when ω is large. The trap centered at $\mathbf{x}_0 = (0.55, 0)$ is one quarter absorbing and three quarters reflecting ($\alpha = 3\pi/4$), with $\omega = 500$ and $\varepsilon = 0.2$. The MFPT is greatest when the absorbing portion is in the rear of the trap (Fig. 7(b)), and is smallest when the absorbing window is at the front of the trap (Fig. 7(d)). In contrast to the stationary case where trap orientation contributes only an $O(\varepsilon)$ quantity to the MFPT, trap orientation is the dominant factor when the rotation speed is large. Note that when the absorbing portion of the trap is oriented towards the center (Fig. 7(a)), the MFPT is low near the center and high in the region between the trap and boundary. The opposite is observed when the absorbing portion is oriented towards the boundary (Fig. 7(c)).
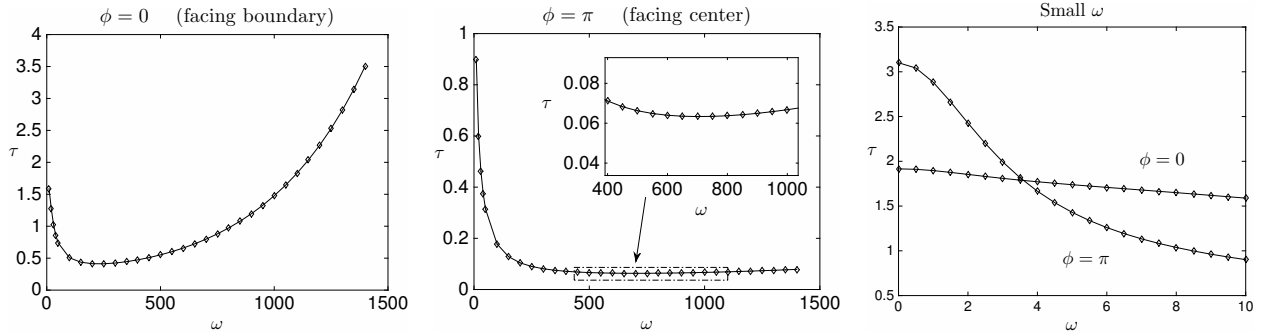

Figure 8: The effect of orientation of a moving trap on the MFPT. In the moving frame, the trap has radius $\varepsilon = 0.2$, $\alpha = 7\pi/8$ (mostly reflecting) and center $\mathbf{x}_0 = (0.55, 0)$. The left panel ($\phi = 0$) shows the MFPT against ω with the absorbing (reflecting) section facing the origin (boundary) while the center panel ($\phi = \pi$) has the absorbing (reflecting) section facing the boundary (origin). The right panel shows that there exists a range of sufficiently small ω for which the $\phi = 0$ orientation generates a larger MFPT than the $\phi = \pi$ case.

To investigate the effect of rotation further, consider a single trap with radius $\varepsilon = 0.2$ inside the unit disk with a single absorbing window that is an eighth of total trap length ($\alpha = 7\pi/8$) so that the absorbing section is relatively small ($|\Gamma_\varepsilon^a|/|\Gamma_\varepsilon^r| = 1/7$). In the rotating frame, the trap is stationary at the point $\mathbf{x}_0 = (0.55, 0)$. We consider two orientation scenarios; first where the Neumann portion is facing the boundary ($\phi = 0$) and the second where it is facing the center of the disk ($\phi = \pi$). In Fig. 8, the MFPT $\tau(\omega) = |\Omega|^{-1} \int_\Omega w(\mathbf{x}; \omega) \, d\mathbf{x}$ obtained from numerical simulation of (4.53) is plotted against ω for each orientation ϕ. There are two primary observations to be made from Fig. 8. First, in each orientation there is a particular rotational speed ω at which the MFPT is minimized. The existence of this minimum may be explained by simply observing that, as $\omega \to \infty$, the reflecting portion of the trap effectively forms a closed reflecting ring, causing the MFPT at all points facing this ring to diverge. Second, a strong shielding effect is observed whereby orientation of the absorbing section towards the boundary ($\phi = \pi$) results in an MFPT that is much smaller than the case $\phi = 0$ when ω is sufficiently large.

As a final example, we examine in additional detail the transition between the optimal orientation condition (3.40) determined in §3.1 for $\omega = 0$ and the new optimal orientations observed in Figs. 7-8. For a single trap with one reflecting portion and $\alpha = 3\pi/4$, we numerically calculate the MFPT τ for several ω as the orientation ϕ is varied over $[0, 2\pi]$. In Fig. 9(a), the $\omega = 0$ curve shows the MFPT to be at a minimum when $\phi = 0$ and maximized when $\phi = \pi$ in agreement with (3.40). As ω increases in value, the location of these extrema migrate before eventually settling on $\phi = \pi/2$ and $\phi = 3\pi/2$ for the maximum and minimum respectively. Interestingly, the approach to the limiting locations of the extrema is seen to be non-monotone in both panels of Fig. 9.

5   Discussion

In this paper we have examined the effect that the orientation of the mixed trap has on the average mean first passage time τ, based on a uniform distribution of starting locations. The result (1.2) gives the expansion of τ to three orders. The first-order $O(1/\log(1/\varepsilon))$ term encodes the information about the area of the
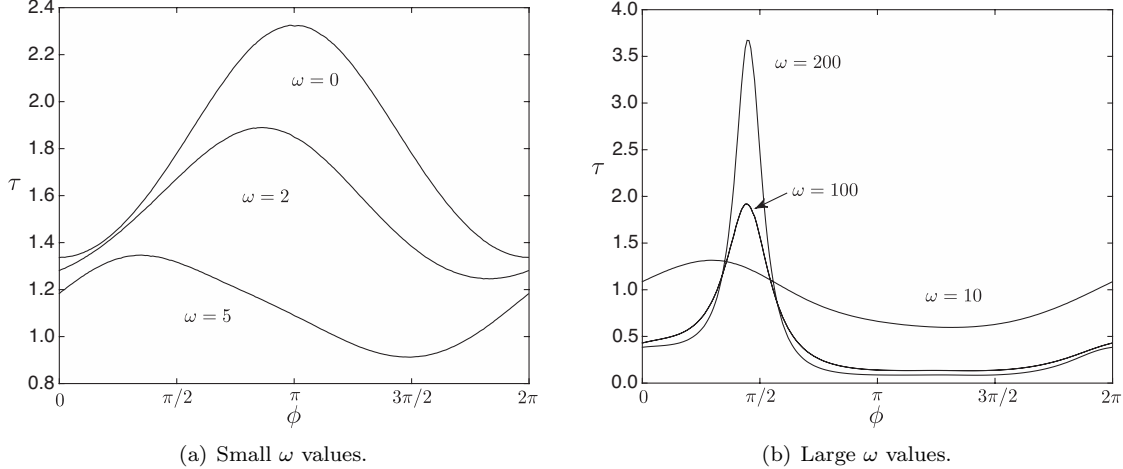
(a) Small ω values. (b) Large ω values.

Figure 9: The effect of orientation ϕ on MFPT τ for the case $\alpha = 3\pi/4$ and several values of angular velocity ω. In the moving frame, the trap is centered at $\mathbf{x}_0 = (0.55, 0)$ with radius $\varepsilon = 0.2$. Curves obtained from numerical simulation of (4.53) on the unit disc.

trap (there is an analogous formula for τ with N traps; in this case, the first-order term would also encode the number of traps). The second-order $O(1)$ term encodes *spatial information*, that is, the position of the trap(s). Finally, the information about trap orientation is encoded in the *third-order $O(\varepsilon)$* term.

The effect of trap orientation depends on two factors: the geometry of the domain (through the gradient of the Neumann's Green's function) and most critically, the alignment vector $(\mathbf{p} + \mathbf{b})$ obtained by solving certain inner problems (2.10) and (2.18). In particular, if this vector is zero, the third-order term in (1.2) is zero, and higher-order (quadrapole) terms must be computed to determine the effect of the orientation. This is the case, for example, for a fully absorbing trap in the form of an oblate ellipse, for which the dipole vector can be computed explicitly using analytic mapping techniques. In particular, it is an open problem to determine the optimal orientation of an ellipse that minimizes τ.

More generally, the dipole vector should be zero for any trap that has at least *two* axes of symmetry. This includes "fragmented" traps such as in Fig. 6. To show this, note that the orientation term in (1.2) can be written in the form $C \cos(\phi - \phi_0)$ where $C \geq 0$ and ϕ_0 are constants and ϕ is the orientation angle (i.e., the trap is rotated through angle ϕ with respect to reference angle ϕ_0). This means that unless $C = 0$, there is exactly *one* optimal orientation $\phi = \phi_0 + \pi$ which minimizes τ. But for ellipses and other traps with high symmetry, there are at least *two* such optimal configurations. We conjecture that for traps with N axes of symmetry, the $O(\varepsilon^N)$ term in the expansion of τ determines the effect of orientation – a very insignificant effect when $N \geq 2$.

The scenario changes dramatically when the trap is rotating. In this case, the trap orientation can have a profound effect on τ as illustrated in Figure 7. In particular, if the absorbing portion is behind the moving trap, the trap itself appears to provide a "shielding effect" and the MFPT tends to infinity as the angular velocity increases. On the other hand, the orientation that minimizes τ is with the absorbing portion in front of the trap. In light of the situation investigated numerically in §4.2, it is apparent that optimization of the MFPT τ over the parameters $(\omega, \varepsilon, \phi, \alpha)$ is a complex problem with many local extrema. Further investigation is needed to better understand this phenomenon.

Acknowledgements

17

Appendix A   The inner problem

In this appendix, we compute the constants a_0, a_1, b_0 as needed in (1.2) and (1.6). To compute the constants a_0, a_1, we seek a harmonic function in the exterior of the unit disk with mixed boundary conditions. First, consider the case $\phi = 0$; the solution when the Neumann (reflecting) boundary section is not centered on the x-axis will be obtained from rotation.

We utilize polar coordinates $\mathbf{y} = r(\cos\theta, \sin\theta)$ for $r = |\mathbf{y}| \geq 1$ and $\theta \in (-\pi, \pi)$ and solve

$$
\begin{cases}
\Delta v = 0, & r \geq 1; \\
\partial_n v = 0, & \theta \in (-\alpha, \alpha); \\
v = 0, & \theta \in (\alpha, \pi) \cup (-\pi, -\alpha); \\
v \sim \quad \log|\mathbf{y}| - \log d_0 + \dfrac{\mathbf{p} \cdot \mathbf{y}}{|\mathbf{y}|^2} + \cdots, & r \to \infty.
\end{cases}
\tag{A.1}
$$

The first step is to write $v = \log r + u$ and solve the associated problem

$$
\begin{cases}
\Delta u = 0, & r \geq 1; \\
\partial_n v = -1, & \theta \in (-\alpha, \alpha); \\
u = 0, & \theta \in (\alpha, \pi) \cup (-\pi, -\alpha); \\
u \sim \quad -\log d_0 + \dfrac{\mathbf{p} \cdot \mathbf{y}}{|\mathbf{y}|^2} + \cdots, & r \to \infty.
\end{cases}
\tag{A.2}
$$

The setup of the problem is such that $u(r, -\theta) = u(r, \theta)$, and so the solution admits a cosine series

$$
u(r, \theta) = \frac{a_0}{2} + \sum_{n=1}^{\infty} \frac{a_n}{r^n} \cos n\theta.
\tag{A.3}
$$

Applying the boundary conditions to the solution (A.3) gives the dual trigonometric series where we need only consider the range $\theta \in (0, \pi)$:

$$
\frac{a_0}{2} + \sum_{n=1}^{\infty} a_n \cos n\theta = 0, \qquad \theta \in (\alpha, \pi);
\tag{A.4a}
$$

$$
\sum_{n=1}^{\infty} n a_n \cos n\theta = 1, \qquad \theta \in (0, \alpha).
\tag{A.4b}
$$

We now seek to determine the coefficients a_n. The solution to this problem is detailed in [32]; see also [33]. For convenience, we outline the main steps here. Consider the representation of the Dirichlet data along the Neumann boundary

$$
g(\theta) = \frac{a_0}{2} + \sum_{n=1}^{\infty} a_n \cos n\theta = \cos\frac{\theta}{2} \int_{\theta}^{\alpha} \frac{h(t) \mathrm{d}t}{\sqrt{\cos\theta - \cos t}}, \qquad \theta \in (0, \alpha),
\tag{A.5}
$$

where $h(t)$ is a function to be determined. The Fourier coefficients a_n are now given by

$$
a_n = \frac{2}{\pi} \int_0^{\alpha} g(\theta) \cos n\theta \, \mathrm{d}\theta = \frac{2}{\pi} \int_0^{\alpha} \cos\frac{\theta}{2} \int_{\theta}^{\alpha} \frac{h(t) \mathrm{d}t}{\sqrt{\cos\theta - \cos t}} \cos n\theta \, \mathrm{d}\theta
$$

$$
= \frac{1}{\pi} \int_0^{\alpha} \left[\int_{\theta}^{\alpha} \frac{h(t)[\cos\theta(n + \frac{1}{2}) + \cos\theta(n - \frac{1}{2})] \, \mathrm{d}t}{\sqrt{\cos\theta - \cos t}} \right] \mathrm{d}\theta.
$$

Changing the order of integration and using the identity

$$
P_n(\cos u) = \frac{\sqrt{2}}{\pi} \int_0^u \frac{\cos\theta(n + \frac{1}{2})}{\sqrt{\cos\theta - \cos u}} \, \mathrm{d}\theta,
\tag{A.6}
$$

18

where $P_n(z)$ is the nth Legendre Polynomial, gives

$$a_0 = \sqrt{2} \int_0^\alpha h(t)\, \mathrm{d}t, \qquad a_n = \frac{1}{\sqrt{2}} \int_0^\alpha h(t)\Big(P_n(\cos t) + P_{n-1}(\cos t) \Big)\, \mathrm{d}t, \qquad n \geq 1. \tag{A.7}$$

These expressions for a_n are now used in the condition (A.4a) generated by the Neumann data. Integrating (A.4a) gives $\sum_{n=1}^\infty a_n \sin n\theta = \theta$, and therefore

$$\frac{1}{\sqrt{2}} \sum_{n=1}^\infty \sin n\theta \int_0^\alpha h(t)\Big(P_n(\cos t) + P_{n-1}(\cos t) \Big)\, \mathrm{d}t = \theta. \tag{A.8}$$

We now employ the key identity

$$\frac{1}{\sqrt{2}} \sum_{n=1}^\infty \sin n\theta \Big(P_n(\cos t) + P_{n-1}(\cos t) \Big) = \frac{\cos\frac{\theta}{2} H(\theta - t)}{\sqrt{\cos t - \cos\theta}},$$

where $H(z)$ is the Heaviside function. This determines the integral equation for $h(t)$,

$$\int_0^\theta \frac{h(t)}{\sqrt{\cos t - \cos\theta}}\, \mathrm{d}t = \theta \sec\frac{\theta}{2}, \tag{A.9}$$

which has the solution

$$h(t) = \frac{2}{\pi}\frac{\mathrm{d}}{\mathrm{d}t} \int_0^t \frac{u \sin\frac{u}{2}}{\sqrt{\cos u - \cos t}}\, \mathrm{d}u. \tag{A.10}$$

We now calculate the logarithmic capacitance to be $d_0 = \exp(-a_0/2)$ where

$$a_0 = \sqrt{2} \int_0^\alpha h(t)\, \mathrm{d}t = \frac{2\sqrt{2}}{\pi} \int_0^\alpha \frac{\mathrm{d}}{\mathrm{d}t}\left[\int_0^t \frac{u \sin\frac{u}{2}}{\sqrt{\cos u - \cos t}}\, \mathrm{d}u \right] \mathrm{d}t$$

$$= \frac{2\sqrt{2}}{\pi} \int_0^\alpha \frac{u \sin\frac{u}{2}}{\sqrt{\cos u - \cos\alpha}}\, \mathrm{d}u. \tag{A.11}$$

For the dipole moment, we determine that

$$a_1 = \frac{1}{\sqrt{2}} \int_0^\alpha h(t)\Big(P_1(\cos t) + p(\cos t) \Big)\, \mathrm{d}t = \frac{1}{\sqrt{2}} \int_0^\alpha h(t)\big(\cos t + 1 \big)\, \mathrm{d}t$$

$$= \frac{\sqrt{2}}{\pi} \int_0^\alpha \frac{\mathrm{d}}{\mathrm{d}t}\left(\int_0^t \frac{u \sin\frac{u}{2}\, \mathrm{d}u}{\sqrt{\cos u - \cos t}} \right)\big(\cos t + 1 \big)\, \mathrm{d}t$$

$$= \frac{\sqrt{2}}{\pi} \left((\cos\alpha + 1) \int_0^\alpha \frac{u \sin\frac{u}{2}}{\sqrt{\cos u - \cos\alpha}}\, \mathrm{d}u + \int_0^\alpha \sin t \left[\int_0^t \frac{u \sin\frac{u}{2}\, \mathrm{d}u}{\sqrt{\cos u - \cos t}} \right] \mathrm{d}t \right). \tag{A.12}$$

Changing the order of integration in the second term of (A.12), integrating once more and recalling the definition of a_0 from (A.11), we obtain that

$$a_1 = a_0 \cos^2\frac{\alpha}{2} + \frac{2\sqrt{2}}{\pi} \int_0^\alpha u \sin\frac{u}{2} \sqrt{\cos u - \cos\alpha}\, \mathrm{d}u. \tag{A.13}$$

We obtain the dipole vector $\mathbf{p}$ for any orientation by rotation

$$\mathbf{p} = \begin{bmatrix} \cos\phi & -\sin\phi \\ \sin\phi & \cos\phi \end{bmatrix} \begin{bmatrix} a_1 \\ 0 \end{bmatrix} = a_1 \begin{bmatrix} \cos\phi \\ \sin\phi \end{bmatrix}. \tag{A.14}$$

Next we compute the solution to the problem (2.18). We write $\mathbf{V}_c = V_1 \mathbf{e}_1 + V_2 \mathbf{e}_2$ and subsequently, the first component admits the series solution

$$V_1 = b_0 + r\cos\theta + \sum_{m=1}^\infty b_m r^{-m} \cos m\theta,$$

where $\mathbf{y} = r(\cos\theta, \sin\theta)$. Applying boundary conditions, the dual series

$$\begin{cases} b_0 + \displaystyle\sum_{n=1}^{\infty} b_n \cos n\theta & = -\cos\theta & \text{on} \quad \theta \in (\alpha, \pi); \\ \displaystyle\sum_{n=1}^{\infty} nb_n \cos n\theta & = \cos\theta & \text{on} \quad \theta \in (0, \alpha), \end{cases} \tag{A.15}$$

is obtained. Following the steps outlined in §A, the value of b_0 is calculated to be

$$b_0 = \frac{2\sqrt{2}}{\pi} \int_0^\alpha \frac{\sin u \sin \frac{u}{2}}{\sqrt{\cos u - \cos\alpha}} \, du. \tag{A.16}$$

Half-absorbing trap. The integrals defining a_0, a_1, b_0 can be evaluated explicitly when $\alpha = \pi/2$. Omitting the details, we obtain

$$a_0 = 2\log 2, \quad a_1 = 1, \quad \text{and} \quad b_0 = 1 \quad \text{when } \alpha = \pi/2. \tag{A.17}$$

Small absorbing trap fraction. Next, we consider the situation where the Dirichlet portion of the trap is very small. This corresponds to the asymptotic regime

$$\alpha = \pi - \mu, \quad \mu \ll 1.$$

The asymptotics of a_0 were derived in [32] in this case. Here we use a different approach (based on singularity analysis, see [34]) to rederive this result and also to derive the asymptotics for a_1 and b_0.

Since the main contribution to (A.11) is near $u = \pi - \mu$, we change variables $u = \pi - \mu - t$ and rewrite

$$a_0 = \frac{2\sqrt{2}}{\pi} \int_0^{\pi-\mu} \frac{(\pi - \mu - t)\cos\frac{\mu+t}{2}}{\sqrt{(\cos\mu)(1 - \cos t) + \sin\mu\sin t}} \, dt.$$

We split the integral $\int_0^{\pi-\mu} = \int_0^\delta + \int_\delta^{\pi-\mu}$, for $\mu \ll \delta \ll 1$ and obtain

$$\int_0^\delta \sim \int_0^\delta \frac{\sqrt{2}\pi}{\sqrt{t^2 + 2\mu t}} dt = \sqrt{2}\pi \log\left(1 + \frac{\delta}{\mu} + \frac{1}{\mu}\sqrt{2\delta\mu + \delta^2}\right) \sim \sqrt{2}\pi \log\left(2\delta/\mu\right),$$

and

$$\int_\delta^{\pi-\mu} \sim \int_\delta^\pi \frac{(\pi - t)\cos\frac{t}{2}}{\sqrt{1 - \cos(t)}} dt \sim \int_\delta^\pi \frac{(\pi - t)\cos\frac{t}{2}}{\sqrt{2}\sin(t/2)} dt$$

$$\sim \int_{\delta/2}^{\pi/2} \frac{\sqrt{2}(\pi - 2s)\cos s}{\sin s} ds$$

$$\sim \sqrt{2}\pi \int_{\delta/2}^{\pi/2} \frac{\cos s}{\sin s} ds - \sqrt{2}\pi \log 2 \qquad \left(\text{using } \int_0^{\pi/2} \frac{s\cos s}{\sin s} ds = \frac{\pi \log 2}{2}\right)$$

$$\sim \sqrt{2}\pi \log \delta^{-1}.$$

Adding the two contributions we therefore obtain

$$a_0 \sim -4\log\frac{\mu}{2} + O(\mu). \tag{A.18}$$

Integrals in b_0 and a_1 have no singularities as $\mu \to 0$. Using the identity $\int_0^{\pi/2} \frac{\sin 2s \sin s}{\cos s} ds = \pi/2$ we obtain

$$a_1 \sim 2, \qquad b_0 \sim 2. \tag{A.19}$$

References

[1] P. C. Bressloff, J. M. Newby, Stochastic models of intracellular transport, Rev. Mod. Phys. 85 (2013) 135–196.

[2] P. C. Bressloff, B. A. Earnshaw, M. J. Ward, Diffusion of protein receptors on a cylindrical dendritic membrane with partially absorbing traps, SIAM Journal on Applied Mathematics 68 (5) (2008) 1223–1246.

[3] M. Titcombe, M. Ward, An asymptotic study of oxygen transport from multiple capillaries to skeletal muscle tissue, SIAM Journal on Applied Mathematics 60 (5) (2000) 1767–1788.

[4] A. Gabel, S. N. Majumdar, N. K. Panduranga, S. Redner, Can a lamb reach a haven before being eaten by diffusing lions?, Journal of Statistical Mechanics: Theory and Experiment 2012 (05) (2012) P05011.

[5] G. Oshanin, O. Vasilyev, P. L. Krapivsky, J. Klafter, Survival of an evasive prey, Proceedings of the National Academy of Sciences 106 (33) (2009) 13696–13701.

[6] L. Mirny, M. Slutsky, Z. Wunderlich, A. Tafvizi, J. Leith, A. Kosmrlj, How a protein searches for its site on DNA: the mechanism of facilitated diffusion, Journal of Physics A: Mathematical and Theoretical 42 (43) (2009) 434013.

[7] O. Bénichou, Y. Kafri, M. Sheinman, R. Voituriez, Searching fast for a target on DNA without falling to traps, Phys. Rev. Lett. 103 (2009) 138102.

[8] D. Coombs, R. Straube, M. Ward, Diffusion on a sphere with localized traps: Mean first passage time, eigenvalue asymptotics, and Fekete points, SIAM Journal on Applied Mathematics 70 (1) (2009) 302–332.

[9] D. Holcman, Z. Schuss, Time scale of diffusion in molecular and cellular biology, Journal of Physics A: Mathematical and Theoretical 47 (17) (2014) 173001.

[10] D. Holcman, Z. Schuss, The narrow escape problem, SIAM Review 56 (2) (2014) 213–257.

[11] R. Metzler, G. Oshanin, S. Redner (Eds.), First-Passage Phenomena and Their Applications, World Scientific, 2014.

[12] O. Bénichou, R. Voituriez, From first-passage times of random walks in confinement to geometry-controlled kinetics, Physics Reports 539 (4) (2014) 225–284.

[13] H. C. Berg, Random Walks in Biology, Princeton University Press, 1993.

[14] S. Redner, A guide to first-passage processes, Cambridge University Press, 2001.

[15] A. Singer, Z. Schuss, D. Holcman, Narrow escape, part ii: The circular disk, Journal of Statistical Physics 122 (3) (2006) 465–489.

[16] S. Pillay, M. Ward, A. Peirce, T. Kolokolnikov, An asymptotic analysis of the mean first passage time for narrow escape problems: Part i: Two-dimensional domains, Multiscale Modeling and Simulation 8 (3) (2010) 803–835.

[17] S. Ozawa, Singular variation of domains and eigenvalues of the Laplacian, Duke Mathematical Journal 48 (4) (1981) 767–778.

[18] T. Kolokolnikov, M. S. Titcombe, M. J. Ward, Optimizing the fundamental Neumann eigenvalue for the Laplacian in a domain with small traps, European Journal of Applied Mathematics 16 (2005) 161–200.

[19] M. Ward, J. Keller, Strong localized perturbations of eigenvalue problems, SIAM Journal on Applied Mathematics 53 (3) (1993) 770–798.

[20] L. Dagdug, A. M. Berezhkovskii, S. Y. Shvartsman, G. H. Weiss, Equilibration in two chambers connected by a capillary, The Journal of chemical physics 119 (23) (2003) 12473–12478.

[21] Z. Schuss, The narrow escape problema short review of recent results, Journal of Scientific Computing 53 (1) (2012) 194–210.

[22] A. Singer, Z. Schuss, D. Holcman, R. Eisenberg, narrow escape, part i, Journal of statistical physics 122 (3) (2006) 437–463.

[23] F. Wei, D. Yang, R. Straube, J. Shuai, Brownian diffusion of ion channels in different membrane patch geometries, Phys. Rev. E 83 (2011) 021919.

[24] E. A. Nigg, Nucleocytoplasmic transport: Signals, mechanisms and regulation, Nature 386 (1997) 779–787.

[25] B. Fahrenkrog, U. Aebi, The nuclear pore complex: Nucleocytoplasmic transport and beyond, Nature Reviews Molecular Cell Biology 4 (10) (2003) 757–766.

[26] A. Cheviakov, M. Ward, R. Straube, An asymptotic analysis of the mean first passage time for narrow escape problems: Part ii: The sphere, Multiscale Modeling & Simulation 8 (3) (2010) 836–870.
URL http://dx.doi.org/10.1137/100782620

[27] M. Ward, W. Heshaw, J. Keller, Summing logarithmic expansions for singularly perturbed eigenvalue problems, SIAM Journal on Applied Mathematics 53 (3) (1993) 799–828.

[28] J.-F. Rupprecht, O. Bénichou, D. Grebenkov, R. Voituriez, Exit time distribution in spherically symmetric two-dimensional domains, Journal of Statistical Physics (2014) 1–39.

[29] S. A. Isaacson, J. Newby, Uniform asymptotic approximation of diffusion to a small target, Phys. Rev. E 88 (2013) 012820.

[30] T. Kolokolnikov, M. J. Ward, Reduced wave Green's functions and their effect on the dynamics of a spike for the Gierer–Meinhardt model, European Journal of Applied Mathematics 14 (05) (2003) 513–545.

[31] J. Tzou, T. Kolokolnikov, Mean first passage time for a small rotating trap inside a reflective disk, SIAM Multiscale Modeling and Simulation .

[32] A. Singer, Z. Schuss, D. Holcman, Narrow escape, part ii: The circular disk, Journal of statistical physics 122 (3) (2006) 465–489.

[33] I. N. Sneddon, Mixed boundary value problems in potential theory, North-Holland, 1966.

[34] E. J. Hinch, Perturbation methods, Cambridge university press, 1991.